Highly sensitive detection of daminozide using terahertz metamaterial sensors

Hanping Mao[1,2*], Xiaoxue Du[1,2], Yuting Yan[1,2], Xiaodong Zhang[1,2], Guoxin Ma[1,2], Yafei Wang[1,2], Yong Liu[1,2], Bin Wang[1,2], Xiaoyue Yang[3], Qiang Shi[1,2]

(1. *Key Laboratory of Modern Agricultural Equipment and Technology, Ministry of Education, Jiangsu University, Zhenjiang 212013, Jiangsu, China*;
2. *School of Agricultural Engineering, Zhenjiang 212013, Jiangsu, China*;
3. *Department of Obstetrics and Gynecology, Affiliated Hospital of Jiangsu University, Zhenjiang 212013, Jiangsu, China*)

Abstract: In order to solve the problems of low sensitivity and complex sample pretreatment in traditional detection, a method was proposed in this study to detect daminozide using terahertz combined with a metamaterial sensor, which enables real-time and label-free molecular detection with high sensitivity. The correlation between the transmission frequency shift and absorbance of daminozide solution at different concentrations was analyzed. The simulation and experimental results showed that this metamaterial sensor could achieve highly sensitive sensing of daminozide solutions at 0.05 mg/L. The maximum quality factor (Q_{max}) of the two peaks could reach 5.78 and 13.05, and the maximum figure of merit (FOM) of the two peaks can reach 0.82 and 1.72. The maximum sensitivity of two resonance peaks reached 38.148 GHz/(mg·L) and 133.516 GHz/(mg·L) when the concentration of daminozide in the solution was 2000 mg/L. There was an obvious positive correlation between the transmission and transmission, frequency shift and frequency shift, and absorbance and absorbance of the resonance peak of daminozide solutions. Therefore, this platform not only opens up new possibilities for the microanalysis of the chemical composition of substances in solutions but also provides a valuable reference for the design of other metamaterial-based sensors in the field of food safety.

Keywords: Terahertz time-domain spectroscopy, plant growth regulator, detection, metamaterial
DOI: 10.25165/j.ijabe.20221506.7600

Citation: Mao H P, Du X X, Yan Y T, Zhang X D, Ma G X, Wang Y F, et al. Highly sensitive detection of daminozide using terahertz metamaterial sensors. Int J Agric & Biol Eng, 2022; 15(6): 180–188.

1 Introduction

Daminozide (succinic acid 2,2-dimethyl hydrazide) is a type of succinic acid plant growth regulator (PGR) with various effects, including bactericidal, and a wide range of applications. It can be used as a dwarfing agent, fruit-setting agent, rooting agent, preservative, etc.[1] However, the abuse of PGRs in agriculture can result in fruits and vegetables containing residual PGRs, which pose potential toxicity to humans[2,3]. Therefore, the convenient, rapid, and sensitive detection of PGR residues is essential to ensure food safety for consumers. As a biomolecule, daminozide has the molecular structure and related environmental information that will produce a terahertz (THz) wave response, and show different absorption positions and intensities. This enables the use of THz spectroscopy to study the structure, configuration, and environmental state of biomolecules.

Nowadays, there is an increasing recognition that THz spectroscopy can be used for high-sensitivity molecular sensing. First, THz spectroscopy can reveal a large amount of molecular structure information, and measure the vibration of low-frequency molecules in intermolecular or intramolecular vibration modes, including hydrogen bonds, van der Waals interactions, and irrelevant (hydrophobic) interactions[4]. In addition, when the millielectron volt (meV) is significantly smaller than the energy of X-ray photons (ranging from ~100 eV to ~100 keV), the ionizing radiation does not influence the radiation energy generated, thus does not affect the properties of the target. Due to their permeability, fingerprint recognition, and security, terahertz time-domain spectroscopy (THz-TDS) and image measurement have great application potential in the agri-food field[5]. However, at THz frequencies, most studies using this technology are usually limited to dry or partially water-containing samples due to the strong absorption of polar liquids (such as water). Since most of the functions of chemical and biological materials are expressed in an aqueous environment, and the water environment is the main solvent of most biological substances, it is necessary to develop an inexpensive sensor platform for real water-based biological

Received date: 2022-04-16 **Accepted date:** 2022-07-22
Biographies: **Xiaoxue Du**, PhD candidate, research interest: intelligent agricultural equipment and technology, Email: dx66610474@163.com; **Yuting Yan**, PhD, Associate Researcher, research interest: intelligent agricultural equipment and technology, Email: yanyuting@ujs.edu.cn; **Xiaodong Zhang**, PhD, Associate Researcher, research interest: intelligent agricultural equipment and technology, Email: zxd700227@126.com; **Guoxin Ma**, PhD, research interest: intelligent agricultural equipment and technology, Email: Gavin_Ma123@163.com; **Yafei Wang**, PhD candidate, research interest: intelligent agricultural equipment and technology, Email: wangyafei918@126.com; **Yong Liu**, PhD candidate, research interest: intelligent agricultural equipment and technology, Email: 2111816007@stmail.ujs.edu.cn; **BinWang**, PhD candidate, Associate Researcher, research interest: intelligent agricultural equipment and technology, Email: 2112016004@stmail.ujs.edu.cn; **Xiaoyue Yang**, PhD candidate, Director, research interest: clinical oncology, Email: xiaoyue_yang_15@163.com; **Qiang Shi**, PhD, Associate Professor, research interest: intelligent agricultural equipment and technology, Email: xyshiqiang@163.com.
***Corresponding author: Hanping Mao**, PhD, Professor, research interest: modern agricultural equipment and environmental control technology of facility agriculture. Department of agricultural equipment, Jiangsu University, Zhenjiang, 212013, Jiangsu, China. Tel: +86-13511695868, Email: maohpujs@163.com.

systems[6,7]. As a result, the combination of THz-TDS and metamaterials for the quick and convenient analysis of compounds in solution has attracted increasing attention.

Metamaterials are composed of shorter-wavelength metals and/or dielectric elements placed periodically and have unique electromagnetic properties such as negative refraction, limited sub-partial focus, and invisibility[8-11]. The research of metamaterials follows the triangular relationship of "structure-component-function". By adjusting the design and size of the structure, the response characteristics of different bands and physical characteristics are achieved[12]. Specific passive and active photoelectric functions can also be achieved through the selection of the cell and base material components. In addition, metamaterials with interstitial structures have strong localization and enhancement fields, and can sensitively detect trace chemical and biological substances. For instance, the detection of fatty acid, saline water, norfloxacin, cells, and pesticides attached to metamaterials has been reported[13-17]. Xu et al.[18] used THz-TDS combined with metamaterial to detect the chlorpyrifos-methyl (CM), and the limit of detection of CM reached 0.204 mg/L, which is lower than the World Health Organization's provisional guideline limit for CM in vegetables. Then, Ye et al.[19] combined metamaterial methods with terahertz spectroscopic technology to achieve 10^6 times the sensitivity of chlorothalonil solution, which demonstrated the potential of metamaterial technology to improve detection capabilities. Therefore, metamaterials provide a novel way for the development of functional materials and the detection of biomolecules. It can be better to realize trace detection of pesticides and other biological molecules.

In recent years, the research direction of metamaterial sensors has gradually turned to microwave absorbers with periodical water structures or multiple-band absorption[20,21]. Xie et al.[22] proposed a four-layer structure with water inclusions and a resonant resin circular ring, which achieved a perfect absorption rate of over 90% in the frequency range from 12.0 to 29.6 GHz. Zhang et al.[23] introduced a four-layer ultra-broadband microwave absorber with a supernatant microstructure, and the results indicated that the absorber could achieve 90% perfect absorption from 4.3 to 40.0 GHz. Later, Han et al.[24] reported a dielectric absorber made from salt water and polytetrafluoroethylene, which had an absorption capacity of over 90% in the frequency bands 1.4-3.3 GHz and 4.3-63.0 GHz and a relative absorption bandwidth of up to 180%. Wang et al.[25] proposed a single and double U-shaped resonator THz metamaterial based on split-ring resonators with multi-frequency resonance achieved. The results show that metamaterial can realize the trace detection of imidacloprid. However, they are difficult to extend to higher frequencies, such as the THz or infrared regions. Moreover, the metamaterial sensor still needs further improvement, in terms of costs, bandwidth, absorption performance, and flexibility.

This study demonstrated the applicability of a double resonance metamaterial as a sensor for the detection of daminozide solutions by spectroscopic analysis in the THz region. First, a dual-resonant metamaterial sensor was designed based on Au-Ti-Polyimide. Then, the variation of the thickness and the refractive index of the surface analyte on the electric field distribution of the metamaterial were analyzed. It could be found that the use of terahertz-TDS could directly and quickly detect daminozide solutions of different concentrations. The results showed that the metamaterials sensor proposed in this study can be used to successfully detect daminozide solutions, as small as 0.05 mg/L. The novel metamaterial sensor has the advantages of highly sensitive and label-free detection, ease of use, and reusability, which opens up a broad prospect for the application of THz label-free sensor in food quality and safety control.

2 Simulation and experimental methods

2.1 Metamaterial design and simulation

The geometric configuration of the designed double-formant metamaterial sensor is shown in Figure 1. In particular, a perspective view of a metamaterial sensor single-cell layout is displayed Figures 1a-1c show the top view and side view of the sensor, respectively. In this study, the Computer Simulation Technology (CST) Studio Suite (Dassault Systèmes Simulia SE, Vélizy-Villacoublay, France) was used to numerically simulate the structure of metamaterial[16]. The material properties of Au, Ti, and Polyimide were referred from Du et al.[26]

In addition, in order to analyze the rationality of the designed metamaterial structure, we simulated the transmission peaks of the inner square structure, the outer square structure, the bimodal structure, and the bimodal structure with a notch in the range of 0-2.1 THz (as shown in Figure 1e). It can be seen from the figure that for the inner square structure, there is no transmission resonance peak in the range of 0-2.1 THz. The reason is mainly due to the small size of the inner structure, and the incident terahertz wave on the surface of the metamaterial structure does not break the electrical neutrality of the inner square structure. Therefore, there is no obvious transmission resonance peak. The outer square structure and the double square structure produce unique resonance peaks around 0.9 THz. It shows that when a terahertz wave is an incident on the outer square structure, the electric neutrality of the inner structure is broken so that the structure produces electric dipoles, and the electric dipoles resonate, which leads to the appearance of resonance peaks. It also shows that the combination of the inner square structure and the outer square structure cannot change the electrical neutrality of the outer square structure. When the gap is designed on one side of the outer square structure, it can be seen that the combination method forms a double resonance transmission peak, which breaks the limitation of the single resonance peak of the metamaterial. It can be seen that the design of the gap in the outer square structure changes the electric field and current inside the metamaterial of the composite structure, resulting in different resonance modes.

To further analyze the influence of the gap (g) size on the resonance peak of metamaterials, the g size of the outer square structure was simulated and optimized (Figure 1f). In the simulation, the size of g was set to be 10 μm, 15 μm, 20 μm, 25 μm, and 30 μm, respectively. When the g gradually increased from 10 to 30 μm, the frequency shifts of both resonance peak 1 and resonance peak 2 gradually shifted to the right, and the transmittance of resonance peak 1 showed a gradually increasing trend. When the g was 30 μm, the transmittance of resonance peak 1 was as high as 96%. However, the transmittance of resonant peak 2 showed a decreasing change with the increase of the g. When the g was 30 μm, the transmittance of resonant peak 2 was 90%, which was 6% lower than that of resonant peak 1. Therefore, considering the difficulty of processing, the size of g as 20 μm was chosen for processing, which not only reduced the processing difficulty but also improved the transmittance of the two resonance peaks.

2.2 Fabrication of the metamaterial

According to the design results, the real metamaterial sensor

samples were also fabricated for experimental measurements. Figure 1d shows the partial microscopic view of the actual metamaterial sensor prepared under an optical microscope. The preparation process mainly includes the following three steps: First, the polyimide layer was spin-coated on a silicon substrate, and baked to imidize the polyimide. Then, the pattern of metamaterial was acquired by standard photolithography (ABM Mask Aligner, ABM Inc. Asia Pacific Ltd., Hong Kong, China) followed by the separate deposition of 10 nm Ti and 200 nm Au layers by electron beam evaporation using a Cook e-beam evaporator (Cooke Vacuum Products, Norwalk, CT, USA). Finally, the whole samples were soaked in the HF solution for 30 min, the polyimide layer with metal metamaterial supported upon would be peeled off from the silicon substrate, and the specimen was divided into 10 mm×10 mm pieces with a Disco cutter (Table S1). Subsequently, the resonant features of flexible metamaterial samples were measured on a TAS7400TS transmissive THz-TDS system (Advantest Corporation, Saitama, Japan).

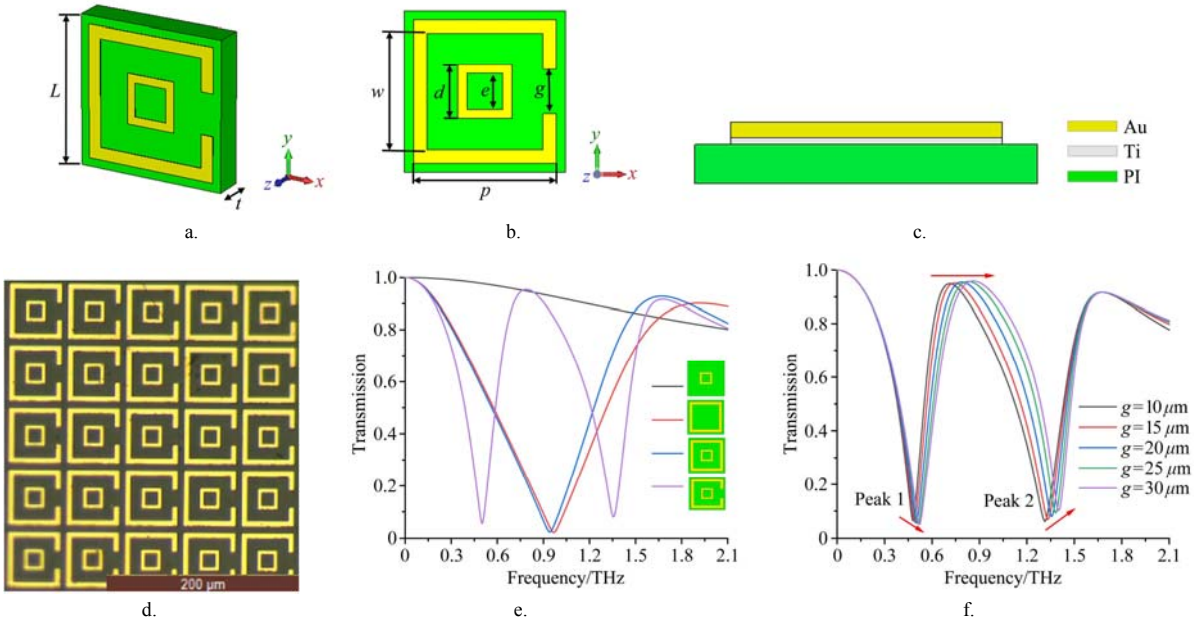

a. b. c. d. e. f.

a. Geometric configuration of the metamaterial sensor b and c. Structural configuration and the top view of the metamaterial sensor, respectively; the parameters are substrate width (L)=72 μm, outer frame metal wire length (p)=64 μm, outer frame metal wire length (w)=52 μm, substrate thickness (t)=14 μm, inner frame metal wire length (d)=24 μm, inner frame metal wire width (e)=16 μm, gap (g)=20 μm d. Partial physical image of the metamaterial sensor e. Resonant peak of different structures f. Resonant peak of the proposed structure for different g size

Figure 1 Schematic diagram and structure optimization diagram of metamaterial sensor

2.3 Experimental method

THz-TDS was used to measure the spectrum using the TAS7400TS transmissive THz-TDS system (Advantest Corporation) in normal transmission detection mode. During the experiment, a frequency resolution of 3.8 GHz was chosen and the frequency range of the acquisition 0.3-2.1 THz was set. In addition, all measurements were performed in a nitrogen atmosphere at a temperature of 25°C±1°C and relative humidity of less than 3%.

Daminozide samples (>99%, BR) were purchased from Dalian Meilum Biotechnology Co., Ltd., Dalian, China. First, the following liquid solutions samples of varying concentrations of daminozide, 0 mg/L, 0.05 mg/L, 0.1 mg/L, 1 mg/L, 5 mg/L, 100 mg/L, 1000 mg/L, and 2000 mg/L, were prepared by dissolving the corresponding amount of the daminozide powder in water. In the experiment of this study, 50 μL of daminozide solutions were dropped on the surface of the metamaterial sensor and allowed to dry (room temperature) before measuring the spectrum of three duplicates. And each spectrum was averaged by three scans.

2.4 Data analysis

In this study, the model proposed by Dorney et al.[27] and Duvillet et al.[28] was used for data processing and optical parameter extraction. After obtaining the reference signal $E_{\mathrm{ref}(t)}$ of the THz time-domain spectrum and the signal $E_{\mathrm{sam}(t)}$ penetrating the sample, fast Fourier transform processing was performed on them separately to obtain the corresponding frequency domain signal amplitudes $E_{\mathrm{ref}(\omega)}$ and $E_{\mathrm{sam}(\omega)}$, and calculate the complex transmission function $H(\omega)$. In addition, a suitable sampling window was selected that included only one THz pulse waveform, and ignored the rest of the echoes, in order to calculate the optical parameters transmittance $T(\omega)$ and absorbance, as follows[29]:

$$T(w)=\frac{E_{out}(w)/P_{sam}(w)}{E_{in}(w)\times P_{air}(w)}=\frac{E_{sam}(w)}{E_{ref}(w)} \quad (1)$$

$$Absorbance(w)=-\log\left|\frac{E_{sam}(w)}{E_{ref}(w)}\right|^2 \quad (2)$$

where, ω is the angular frequency, rad/s; $E_{\mathrm{out}}(\omega)$ is the outgoing electric field; $E_{\mathrm{in}}(\omega)$ is the incident electric field; $T(\omega)$ is the transmittance; $E_{\mathrm{ref}(\omega)}$ is the terahertz wave of the penetrating air; $E_{\mathrm{sam}}(\omega)$ is the terahertz wave of the penetrating of sample; $P_{\mathrm{air}}(\omega)$ and $P_{\mathrm{sam}}(\omega)$ are the transmission factors of terahertz wave in air and sample, respectively.

3 Results and discussion

3.1 Analysis of the simulation results

The transmission spectra of the metamaterial-based sensor were simulated and experimentally measured (Figure 2a). There were two clear resonance peaks at 0.50 and 1.36 THz. The spectra also show that there is a certain level of discrepancy between experimental and simulation results. The main reasons include two aspects. On the one hand, the difference between the simulated conditions and the actual conditions used, and on the other hand the processing errors in the experimental. Thus, there is a difference in the intensity of the resonant peak, and the

resonant frequency deviates. The actual prepared dimensions can be found in Table 1.

Table 1 Structural parameter for the actual preparation of experiment (μm)

Parameter	Value
Substrate width L	72.00
Outer frame metal wire length p	64.62
Outer frame metal wire width w	51.40
Inner frame metal wire length d	24.67
Inner frame metal wire width e	15.39
Gap g	19.39
Substrate thickness t	14.00

In order to determine the transmission mechanism of the transmission peak of the metamaterial sensor, the distributions of the electric field and magnetic field at different resonance frequencies were simulated and analyzed. The electric energy density and the surface currents distribution of the two resonant peaks in the x-y plane were the first investigated. For peak 1, the electric fields were strongly enhanced on the left of the outside of the metal (Figure 2b). Additionally, also it was also found that the surface current was mainly distributed on the left of the outside of the metal, and the surface current of the outer and inner metal frames was in the same direction, that is, the dipole-like parallel currents in Figure 2c. For peak 2, the electric fields were strongly enhanced on the outside of the metal (Figure 2d). The surface current was mainly distributed on the outside of the metal and the surface current of the outer metal frame was in the opposite direction to that of the inner metal frame, that is, the Fano-like antiparallel currents in Figure 2e. These results indicate that the resonance peaks are mainly caused by the uneven distribution of the magnetic field energy due to the different directions of the surface currents. In addition, other researches[30,31] have found that when the geometric parameters of the metamaterial structure were determined, the resonance frequency was related to the surface dielectric environment and electric field, which is consistent with the conclusion of this study.

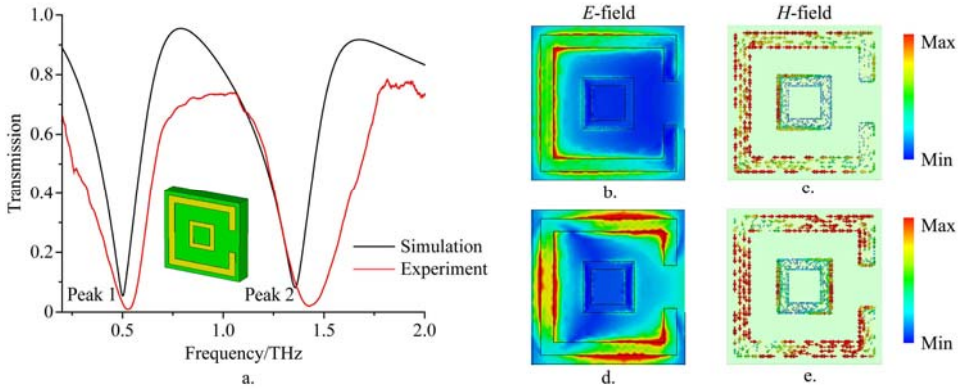

a. Transmission curves obtained by simulation and experiment b and c. Corresponding electric field, magnetic field, and surface current distribution on top at the resonant frequencies of 0.5 THz. d and e. Corresponding electric field, magnetic field, and surface current distribution on top at the resonant frequencies of 1.36 THz.

Figure 2 Transmission diagram of metamaterial sensor and the electric field and surface current distribution of its corresponding resonance peak

To theoretically model the spectral response of the metamaterial sensor with a thin-film analyte on its surface, the transmission spectral response of the metamaterial sensor was investigated with different analyte thicknesses. Figure 3a shows the variation of the simulated spectral transmission amplitude with the thickness of the analyzed layer when the thickness of the analyte on the surface of the metamaterial is in the range of 0-15 μm. The results show that as the thickness of the analyte increases, the transmission peak shifts to the low-frequency direction. When the thickness of the measured object increases from 0 to 15 μm, the frequency of the resonance peak 1 of the metamaterial sensor increases from 0.50 to 0.40 THz, the displacement is 19.5%, and the sensitivity is 6.5 GHz/μm. In addition, when the thickness of the measured object increases from 0 to 15 μm, the frequency of the resonance peak 2 of the metamaterial sensor increases from 1.36 to 1.11 THz, the frequency shift is 18.39%, and the sensitivity is 16.67 GHz/μm. The simulation results showed that the transmission amplitude of the metamaterial sensor is related to the thickness of the analyte. Furthermore, the frequency shift Δf of the metamaterial-based sensor was analyzed with different analyte thicknesses, as shown in Figure 3c. The analysis revealed that the frequency shift Δf of the resonance peak 1 increased with the increase of the analyte thickness. In particular, when the analyte thickness was 13 μm, the frequency shift Δf occurred at the highest point, that is, the frequency shift Δf was 97.5 GHz. Also, with the increase of the analyte thickness, the frequency redshift Δf of the resonance peak 2 increased at first and then tended to level off. The frequency shift position was the same as that of the resonance peak 1. When the analyte thickness was 13 μm, the frequency shift Δf occurred at the highest point, that is, the frequency shift Δf was 257.5 GHz. Thus, we concluded that the frequency shift of the metamaterial sensor is related to the thickness of the analyte. However, there must be a limit value for Δf. If it exceeds this value, regardless of how large the thickness is, the Δf would not increase significantly anymore[16]. A similar case has also been observed in other studies[32]. Figure 3b shows the spectral transmission amplitude change of the simulated metamaterial surface in the range of refractive index 1.0-1.9, revealing that increasing the refractive index, leads to the resonance peaks being accompanied by a redshift. Compared with resonance peak 1, the red shift of resonance peak 2 is more obvious, indicating that the reflection index has a greater effect on resonance peak 2. This result is the same as that shown in Figure 2a. Further combining the electric field intensity with the current distribution, revealed that the refractive index affects the electric field intensity and surface current distribution. The sensitivity S was the derivative of the Δf-n, which was defined as the degree of change in the sensor's response to changes in the unit amount of analyte[32,33]. The only factor that affects the sensitivity of metamaterial THz sensors is the change in the refractive index of the surface analyte (*i.e.*, frequency shift). As the refractive index

increases gradually, S increases approximately linearly (Figure 3d). When the refractive index was n=1.9, the maximum sensitivity S of resonance peak 1 was 108 GHz/refractive index unit (RIU), and the maximum sensitivity of resonance peak 2 was 286 GHz/RIU. This result indicates that the stronger the magnetic field and the more current distribution, the higher the sensitivity of the sensor. The Fano-like antiparallel currents and the dipole-like parallel currents also have some effect on sensitivity.

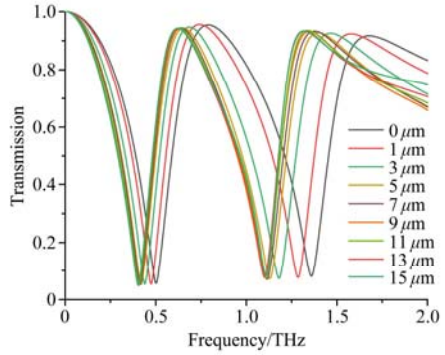

a. Transmission spectral response of the metamaterial sensor with different analyte thickness

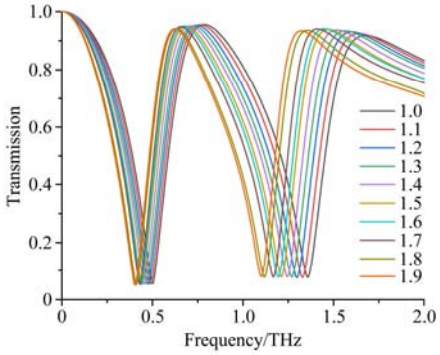

b. Transmission spectral response of the metamaterial sensor with different refractive index

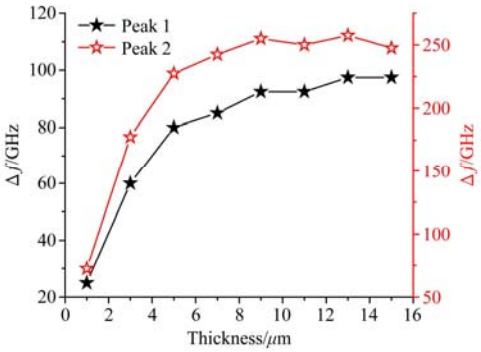

c. Frequency shift Δf of the analyte as extracted from a

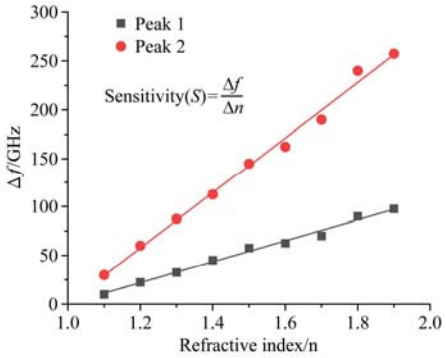

d. Frequency shift Δf of the refractive index as extracted from b

Figure 3 Sensing principle of the metamaterial sensor

3.2 Analysis of experimental results

The sensing performance of the proposed metamaterial was evaluated (Figure 4a) using daminozide, a type of succinic acid plant growth regulator, as an example. The transmission spectra of different solutions of daminozide in water concentrations of 0, 0.05 mg/L, 0.1 mg/L, 1 mg/L, 5 mg/L, 100 mg/L, 1000 mg/L, and 2000 mg/L were measured and are shown in Figure 4b. The spectra reveal the overall trend that the transmittance decreases with increasing daminozide concentration. In addition, they also show that the resonance frequency redshifts of the two peaks were different. Compared with resonance peak 1, the sensing results of resonance peak 2 showed a more remarkable change of transmittance, which is clearly distinct between different daminozide concentrations. This result also confirmed that the coincidence degree between the daminozide transmission peak and metamaterial resonant frequency plays the dominant role.

To illustrate it better, the frequency shift Δf was defined to describe the absolute values of the peak frequency distance between the double-resonance metamaterial resonator curves with and without the analyzed layer, and the results are shown in Figure 4c. For the resonance peak 1, higher frequency shift Δf values (from 0 to 38.148 GHz) were obtained when the concentration of the daminozide solution was increased from 0 to 2000 mg/L. Also, as the daminozide concentration increased, the frequency shift Δf of the resonance peak 2 increased from 0 to 133.516 GHz. The frequency shift results of the two resonance peaks were consistent with the change law of experimental transmission. In our experiment, the sensitivity was defined as $S = \Delta f/\Delta c$[13], where Δc represents the change of the daminozide concentration, and the maximum sensitivity reached 38.148 GHz/mg·L at 2000 mg/L. This means that the resonance peak 1 was shifted 38.148 GHz/mL of daminozide. Regarding resonance peak 2, the maximum sensitivity approached 133.516 GHz/(mg·L) at 2000 mg/L. The results showed that the concentration of daminozide determines the detection sensitivity of the metamaterial sensor, not that the higher the concentration of the sample, the higher the detection sensitivity. Moreover, the resonant peaks at 0.05 mg/L are 0.511 and 1.385 THz, which are different from the resonance peaks at 0 mg/L. That is, the two resonant peaks' frequency redshift at 0.05 mg/L are 15.258 and 49.586 GHz. Thus, the minimum daminozide concentration detected by the metamaterial is 0.05 mg/L, having a better sensitivity than those in previously reported studies using THz-DTS[34]. In addition, the THz time domain spectrogram, shown in Figure 4d, reveals that with the increase of the concentration of daminozide, the amplitude time-shifted successively to the right, indicating that with the increase of the concentration of daminozide, the amplitude time of the samples showed a delayed increase. This result indicates that the combination of metamaterial and THz radiation also has a certain influence on time-domain signals.

As is well known, each metamaterial substance has its unique fingerprint spectrum[30]. This study found that by inducing the field enhancement of the metamaterial, the external field can interact more effectively with the substance being detected when the fingerprint resonance peak of the substance and characteristic spectral peak of the metamaterial structure are close to each other. We detected the characteristic fingerprint peaks of daminozide as shown in Figures 4e and 4f. They revealed that daminozide has 2 distinct characteristic peaks in the 0-2 THz range, namely characteristic peak 1 and characteristic peak 2, which are at

0.45-0.55 THz and 1.2-1.5 THz, respectively. This phenomenon further verifies that in the concentration range of 0.05-2000 mg/L, the coincidence degree between the daminozide fingerprint peak and the structurally characteristic peak of the metamaterial plays a dominant role, which is consistent with previous reports[30,35]. As shown in Figure 4g, when the concentration of daminozide increases from 0.05 to 2000 mg/L, all the characteristic peaks show an initial decreasing trend, followed by an increasing trend and then a decreasing trend again. These results are consistent with the recorded transmission spectra, indicating that the transmission of daminozide is inversely proportional to the absorption at the same concentration, that is, the greater the transmittance of daminozide, the smaller the absorption. The above results also demonstrated that the THz-TDS technique combined with a metamaterial sensor can be used to effectively quantitatively analyze trace substances.

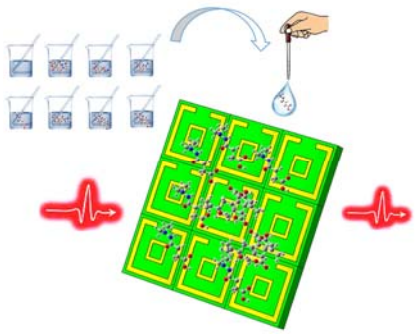

a. Daminozide concentrations detection ability of the metamaterial sensor

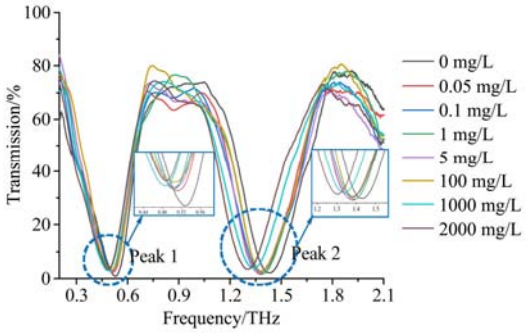

b. The transmission spectra of daminozide solutions

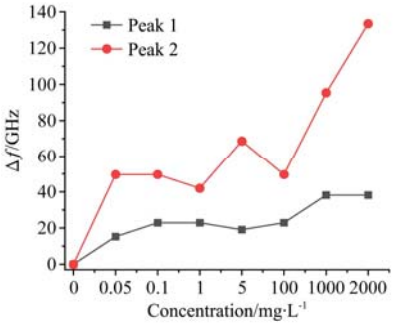

c. Resonant peaks shift Δ*f* of daminozide solutions

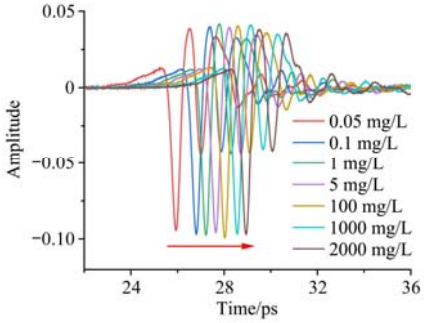

d. THz time domain spectra of liquid samples

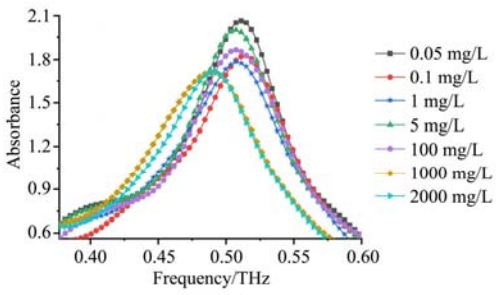

e.

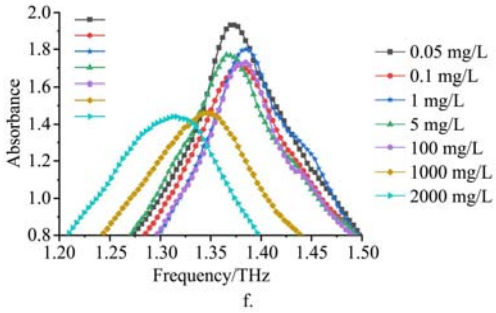

f.

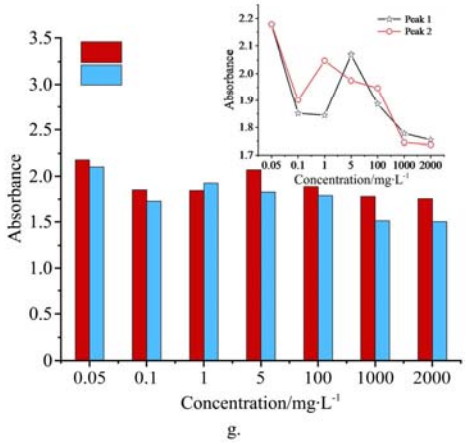

g.

e-g. Absorbance spectra of the daminozide solutions based on metamaterial sensor

Figure 4 Detection ability of daminozide solutions using the metamaterial sensor

In order to further analyze whether there is a correlation between the parameters of the two resonance peaks. The correlations among transmission, frequency shift, and absorbance of the daminozide at different concentrations were analyzed using a robust open-source software platform[36]. As shown in Figure 5, there is an extremely significant positive correlation between absorption peak 1 and absorption peak 2, and the correlation coefficient is 0.82. There is also a significant positive correlation between transmission peak 1 and transmission peak 2, and between the frequency of resonance peak 1 and the frequency shift of resonance peak 2, with correlation coefficients of 0.74 and 0.84, respectively. In addition, there is a positive correlation between transmission peak and frequency shift, indicating that the greater the transmission of daminozide solutions, the more obvious the

frequency shift Δf. Further, it could be achieved that highly sensitive detection of terahertz metamaterial sensors by superimposing the sensing characteristic parameters of the two resonance peaks in the future.

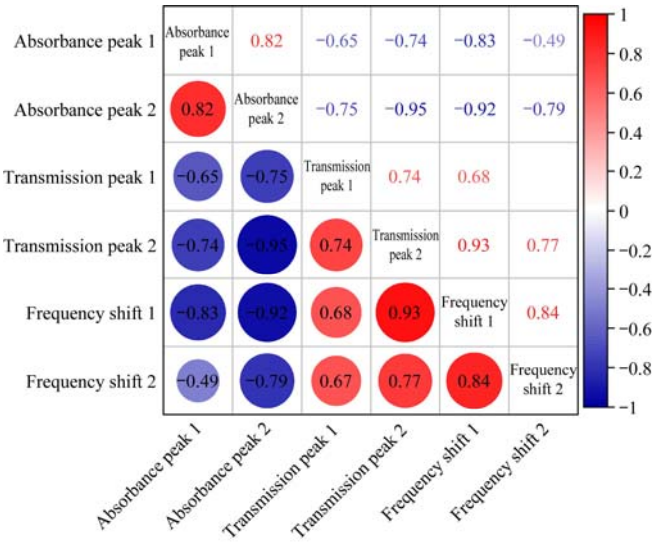

Figure 5 Correlation among transmission, frequency shift, and absorbance of the daminozide at different concentrations

3.3 Comparison of performance indicators

It is useful to compare the sensitivity, advantages, and disadvantages of the biosensor platform developed in this study with those of other label-free biosensor platforms[37]. In general, the values of three parameters are used to evaluate the sensing performance of metamaterial THz sensors[38-40]. The first parameter is the quality factor (Q), which represents the resonance characteristics of the sensor. The Q value is related to the resolution and sensitivity of the sensor. Under the same other conditions, as the Q value of the sensor increases, its resolution also increases. In the case of the same resolution, a sensor with a higher Q value and a sharper spectral curve has higher sensitivity. The second parameter is sensitivity S, which is the degree of change in the response of the sensor to the change in the unit amount of analyte. The third parameter is the FOM value, a value that represents the sensor performance index. When the sensitivity S is the same, the higher the FOM value, the better the sensing performance of the sensor. As is well established, high Q and FOM values result in a sharper resonance peak, which makes it easier to observe the resonance peak shift[30]. In our experiment, the maximum Q value of the two resonance peaks are 5.78 and 13.05 and the maximum FOM values of the two resonance peaks are 0.82 and 1.72, which are higher than the values in the reference (as shown in Table 2)[30,41]. Although the Q, FOM, and sensitivity values of our design are lower than those reported in the literature[33,42,43], the metamaterial of this study achieved a detection limit of 0.05, while those reported in the literature are not experimentally detected values, but rather are theoretical values obtained from the simulation stage. In the future, the structure of metamaterial was planned to further optimize while improving the Q, FOM, and sensitivity values.

Table 2 Performance comparison of different sensors

The origin of the article	Concentration detection limit	The quality (Q) factor	Sensitivity	Figure of merit (FOM)	Year
Ye et al.[30]	0.1 mg/L	3.6	156 GHz/RIU	0.38	2021
Wang et al.[33]	-	14.2	243 GHz/RIU	3.3	2020
Lin et al.[41]	0.1 ng/mL	--	76.5 GHz/RIU	--	2021
Saadeldin et al.[42]	--	22.05	300 GHz/RIU	2.94	2019
Gupta et al.[43]	--	10	180 GHz/RIU	--	2020
This study	0.05 mg/L	5.78 13.05	108 GHz/RIU 286 GHz/RIU	0.82 1.72	2021

4 Conclusions

In this study, an Au-Ti-Polyimide-based metamaterial sensor was designed, fabricate, and evaluated for the detection of daminozide in solution. Compared with the previously reported THz sensor technology, this novel approach does not require tablet samples, which is more convenient and direct. The simulation and experimental results both confirmed that this method achieved highly sensitive sensing of daminozide in solution at a concentration as low as 0.05 mg/L. Its maximum Q of two peaks can reach 5.78 and 13.05, and the maximum FOM of two peaks can reach 0.82 and 1.72. Correlation analysis showed that there are obvious positive correlations between the transmission and transmission, frequency shift and frequency shift, and absorbance and absorbance of the two resonance peaks in the daminozide solution, and the correlation coefficients are 0.71, 0.84, and 0.82, respectively. This new metamaterial sensor could realize the rapid and efficient detection of daminozide. However, only one plant growth regulator was tested in this study. In future work, the designed metamaterial sensor will be tried to be used to detect other kinds of plant growth regulators or pesticides. It is expected to provide a new detection technology for the field of food detection.

Acknowledgements

The authors gratefully acknowledge that this work was financially supported by the National Natural Science Foundation of China (Grant No. 32071905; No. 62101217; No. 61771224), the Natural Science Foundation of Jiangsu Province (Grant No. BK20190858), the Project of Agricultural Equipment Department of Jiangsu University (Grant No. NZXB20210106), China Postdoctoral Science Foundation (Grant No. 2019M661754), China Scholarship Council (Grant No. 201908320223), Postgraduate Research & Practice Innovation Program of Jiangsu Province (Grant No. KYCX19_1619), and Zhenjiang Science and Technology Innovation Fund (Grant No. SH2020051).

[References]

[1] Wang M G, Nie H L, Han D D, Qiao X Q, Yan H Y, Shen S G. Cauliflower-like resin microspheres with tuneable surface roughness assolid-phase extraction adsorbent for e ffi cient extraction and determination of plant growth regulators in cucumber. Food Chemistry, 2019; 295: 259–266.

[2] Yan H Y, Wang F, Han D D, Yang G L. Simultaneous determination of four plant hormones in bananas by molecularly imprinted solid-phase extraction coupled with high performance liquid chromatography. Analyst, 2012; 137: 2884–2890.

[3] Han Y H, Wang Z Q, Jia J, Bai L G, Liu H Y, Shen S G, et al. Newly designed molecularly imprinted 3-aminophenol-glyoxal-urea resin ashydrophilic solid-phase extraction sorbent for specific simultaneous determi-nation of three plant growth regulators in green bell peppers. Food Chemistry, 2020; 31: 125999. doi: 10.1016/j.foodchem.2019.125999.

[4] Zhao R, Zou B, Zhang G L, Xu D Q, Yang Y P. High-sensitivity identification of aflatoxin B1 and B2 using terahertz time-domain spectroscopy and metamaterial-based terahertz biosensor. Journal of Physics D: Applied Physics, 2020; 53(19): 195401. doi: 10.1088/1361-6463/ab6f90.

[5] Sun X D, Liu J B. Measurement of plumpness for intact sunflower seed using Terahertz transmittance imaging. Journal of Infrared, Millimeter, and Terahertz Waves, 2020; 41(3): 307–321.
[6] Chen M, Singh L, Xu N N, Singh R N, Zhang W L, Xie L J. Terahertz sensing of highly absorptive water-methanol mixtures with multiple resonances in metamaterials. Optics Express, 2017; 25(13): 14089–14097.
[7] Pang Y, Wang J, Cheng Q, Xia S, Zhou X Y, Xu Z, et al. Thermally tunable water-substrate broadband metamaterial absorbers. Applied Physics Letters, 2017; 110(10): 104103. doi: 10.1063/1.4978205.
[8] Shelby R A, Smith D R, Schultz S. Experimental verification of a negative index of refraction. Science, 2001; 292(5514): 77–79.
[9] Liu Z W, Lee H, Xiong Y, Sun C, Zhang X. Far-field optical hyperlens magnifying sub-diffraction-limited objects. Science, 2007; 315(5819): 1686–1686. doi: 10.1126/science.1137368.
[10] Smolyaninov I I, Hung Y J, Davis C C. Magnifying superlens in the visible frequency range. Science, 2007; 315(5819): 1699–1701.
[11] Schurig D, Mock J J, Justice B J, Cummer S A, Pendry J B, Starr A F, et al. Metamaterial electromagnetic cloak at microwave frequencies. Science, 2006; 314(5801): 977–980.
[12] Yi Z, Huang J, Cen C L, Chen X F, Zhou Z G, Tang Y J, et al Nanoribbon-ring cross perfect metamaterial graphene multi-band absorber in THz range and the sensing application. Results in Physics, 2019; 14: 102367. doi: 10.1016/j.rinp.2019.102367.
[13] Tang M J, Xia L P, Wei D S, Yan S H, Zhang M K, Yang Z B, et al. Rapid and label-free metamaterial-based biosensor for fatty acid detection with terahertz time-domain spectroscopy. Spectrochimica Acta Part A: Molecular and Biomolecular Spectroscopy, 2020; 228: 117736. doi: 10.1016/j.saa.2019.117736.
[14] Zhou R Y, Wang C, Huang Y X, Huang K, Wang Y L, Xu W D, et al. Lable-free terahertz microfluidic biosensor for sensitive DNA detection using graphene-metasurface hybrid structures. Biosensors and Bioelectronics, 2021; 188: 113336. doi: 10.1016/j.bios.2021.113336.
[15] Li B, Bai J P, Zhang S J. Low concentration noroxin detection using terahertz spectroscopy combined with metamaterial. Spectrochimica Acta Part A: Molecular and Biomolecular Spectroscopy, 2021; 247: 119101. doi: 10.1016/j.saa.2020.119101.
[16] Yan X, Yang M S, Zhang Z, Liang L J, Wei D Q, Wang M, et al. The terahertz electromagnetically induced transparency-like metamaterials for sensitive biosensors in the detection of cancer cells. Biosensors and Bioelectronics, 2019; 126: 485–492.
[17] Xu W D, Huang Y X, Zhou R Y, Wang Q, Yin J F, Kono J, et al. Metamaterial-free flexible graphene-enabled Terahertz sensors for pesticide detection at bio-interface. ACS Applied Materials & Interfaces, 2020; 12: 44281–44287.
[18] Xu W D, Xie L J, Zhu J F, Wang W, Ye Z Z, Ma Y G, et al. Terahertz sensing of chlorpyrifos-methyl using metamaterials. Food Chemistry, 2017; 218: 330–334.
[19] Ye Y X, Zhang Y X, Zhao Y, Ren Y P, Ren X D. Sensitivity influencing factors during pesticide residue detection research via a terahertz metasensor. Optics Express, 2021; 29(10): 15255–15268.
[20] Shen Y, Zhang J Q, Pang Y Q, Wang J F, Ma H, Qu S B. Transparent broadband metamaterial absorber enhanced by water-substrate incorporation. Optics Express, 2018; 26(12): 15665. doi: 10.1364/OE.26.015665.
[21] Yoo Y J, Ju S, Park S Y, Kim Y J, Bong J, Lim T, et al. Metamaterial absorber for electromagnetic waves in periodic water droplets. Scientific Reports, 2015; 5(1): 14018–14025. doi: 10.1038/srep14018.
[22] Xie J W, Zhu W R, Rukhlenko I D, Xiao F J, He C, Geng J P, et al. Water metamaterial for ultra-broadband and wide-angle absorption. Optics Express, 2018; 26(4): 5052–5059.
[23] Zhang J Q, Wu X Y, Liu L Y, Huang C, Chen X Y, Tian Z, et al. Ultra-broadband microwave metamaterial absorber with tetramethylurea inclusion. Optics Express, 2019; 27(18): 25595–25602.
[24] Xiong H, Yang F. Ultra-broadband and tunable saline water-based absorber in microwave regime. Optics Express, 2020; 28(4): 5306–5316.
[25] Wang Q, Yin S, Shi X D, Fan J C, Huang K, Gao W L, et al. High‐sensitivity detection of trace imidacloprid and tetracycline hydrochloride by multi‐frequency resonance metamaterials. Journal of Food Measurement and Characterization, 2022; 16: 2041–2048.
[26] Du X X, Zhang X D, Wang Y F, Ma G X, Liu Y, Wang B, et al. Highly sensitive detection of plant growth regulators by using terahertz time-domain spectroscopy combined with metamaterials. Optics Express; 2021; 29: 36535. doi: 10.1364/OE.437909.
[27] Dorney T D, Baraniuk R G, Mittleman D M. Material parameter estimation with terahertz time-domain spectroscopy. Journal of the Optical Society American A, 2001; 18: 1562–1571. doi: 10.1364/JOSAA.18.001562.
[28] Duvillaret L, Garet F, Coutaz J L. A reliable method for extraction of material parameters in terahertz time-domain spectroscopy. IEEE Journal of Selected Topics in Quantum Electronics, 1996; 2: 739–746.
[29] Chen T, Zhang Q, Li Z, Yin X H, Hu F R. Experimental and theoretical investigations of tartaric acid isomers by terahertz spectroscopy and density functional theory. Spectrochimica Acta Part A: Molecular and Biomolecular Spectroscopy, 2018; 205: 312–319.
[30] Ye Y X, Zhang Y X, Zhao Y, Ren Y P, Ren X D. Sensitivity influencing factors during pesticide residue detection research via terahertz metasensor. Optics Express, 2021; 29 (10): 15255–15268. doi: 10.1364/OE.424367.
[31] Yan X, Zhang X, Liang L, Yao J. Research progress on the application of terahertz-band metamaterials in biosensors. Spectroscopy and Spectral Analysis, 2014; 34: 2365–2371.
[32] Zhao T G, Yu S L. Ultra-high sensitivity nanosensor based on multiple fano resonance in the MIM coupled plasmonic resonator. Plasmonics, 2017; 13(4): 1115–1120.
[33] Saadeldin A, Hameed M, Elkaramany E, Obayya S. Highly Sensitive Terahertz Metamaterial Sensor. IEEE Sensors Journal, 2019; 19: 7993–7999.
[34] Du X X, Wang Y F, Zhang X D, Ma G X, Liu Y, Wang B, et al. A study of plant growth regulators detection based on terahertz time-domain spectroscopy and density functional theory. RSC advance, 2021; 11: 28898–28907.
[35] Guo X Y, Zhang Z, Yang M S, Bing P B, Yan X, Yang Q L, et al. Time-frequency double domain resolving by electromagnetically induced transparency metasensors for rapid and label-free detection of cancer biomarker midkine. Optics and Lasers in Engineering, 2021; 142: 106566. doi: 10.1016/j.optlaseng.2021.106566.
[36] R-project. Available: http://www.r-project.org. Accessed on [2021-12-01].
[37] O'Hara J F, Singh R J, Brener I, Smirnova E, Han J Q, Taylor A J, et al. Thin-film sensing with planar terahertz metamaterials: sensitivity and limitations. Optics Express, 2008; 16: 1786–1795.
[38] Xu W D, Xie L J, Zhu J F, Xu X, Ye Z Z, Wang C, et al. Gold nanoparticle-based Terahertz metamaterial sensors: Mechanisms and Applications. ACS Photonics, 2016; 3: 2308–2314.
[39] Yi Z, Huang J, Cen C L, Chen X F, Zhou Z G, Tang Y J, et al. Nanoribbon-ring cross perfect metamaterial graphene multi-band absorber in THz range and the sensing application. Results in Physics, 2019; 14: 102367. doi: 10.1016/j.rinp.2019.102367.
[40] Srivastava Y K, Cong L Q, Singh R J. Dual-surface flexible THz Fano metasensor. Applied Physics Letters, 2017; 111: 201101. doi: 10.1063/1.5000428.
[41] Lin S J, Xu X L, Hu F R, Chen Z C, Wang Y L, Zhang L H, et al. Using antibody modified Terahertz metamaterial biosensor to detect concentration of carcinoembryonic antigen. IEEE Journal of Selected Topics in Quantum Electronics, 2021; 27: 6900207. doi: 10.1109/JSTQE.2020.3038308.
[42] Gupta M, Singh R. Terahertz sensing with optimized Q/V metasurface cavities. Advanced Optical Materials, 2020; 8: 1902025. doi: 10.1002/adom.201902025.
[43] Wang Z Y, Geng Z X, Fang W H. Exploring performance of THz metamaterial biosensor based on flexible thin-film. Optics Express, 2020; 28(18): 26370–26384. doi: 10.1364/OE.402222.

Appendix

Table S1 Detailed production process

Step	Number	Name	Condition	Time	Equipment
Spin coating of PI	1	Subtract	Four-inch high-resistance silicon		
	2	Spin-on Coating	Positive rotation 600 r/min Counter rotation 1000 r/min	7 s 30 s	Meitu Semiconductor Coater RC-150
	3	Pre-bake	120°C	5 min	Meitu programmable hot plate PHP-8
	4	Repeat steps 2 and 3 twice			
	5	Imidize the PI	120°C 200°C 250°C	1.0 h 2.0 h 2.5 h	
Lithography	1	Spin-on Coating	Positive rotation 600 r/min Counter rotation 1000 r/min	7 s 30 s	Meitu Semiconductor Coater RC-150
	2	Pre-bake	110°C	2 min	Meitu programmable hot plate PHP-8
	3	UV exposure	9.9 mw/cm^2	4 s	MA6
	4	Hard bake	110°C	2 min 30 s	Meitu programmable hot plate PHP-8
	5	Development	TMAH3038	50 s	
Coating film	1	Coating film	O_2 Plasma 200 W	2 min	March glue
	2	Metallized	Ti 10 nm Au 200 nm		Electron beam evaporation COOK
Lift-off	1	Acetone was used for 5 min to peel off the specimen			
Scribing	1	Coating film	O_2 Plasma 200 W	2 min	March glue
	2	Metallized	Ti 10 nm Au 200 nm		Electron beam evaporation COOK
Separation	1	Soked in HF for 30 min.			